

Sparse Optimization for Robust and Efficient Loop Closing

Yasir Latif^a, Guoquan Huang^b, John Leonard^c, José Neira^d

^aARC Center for Robotic Vision, University of Adelaide, Adelaide SA 5005, Australia¹

^bDepartment of Mechanical Engineering, University of Delaware, Newark, DE 19716, USA

^cComputer Science and Artificial Intelligence Laboratory Massachusetts Institute of Technology, Cambridge, MA 02139, USA

^dInstituto de Investigación en Ingeniería de Aragón (I3A) Universidad de Zaragoza, Zaragoza, Spain

Abstract

It is essential for a robot to be able to detect revisits or *loop closures* for long-term visual navigation. A key insight explored in this work is that the loop-closing event inherently occurs sparsely, i.e., the image currently being taken matches with only a small subset (if any) of previous images. Based on this observation, we formulate the problem of loop-closure detection as a *sparse, convex ℓ_1* -minimization problem. By leveraging fast convex optimization techniques, we are able to efficiently find loop closures, thus enabling real-time robot navigation. This novel formulation requires no offline dictionary learning, as required by most existing approaches, and thus allows *online incremental* operation. Our approach ensures a *unique* hypothesis by choosing only a single globally optimal match when making a loop-closure decision. Furthermore, the proposed formulation enjoys a *flexible* representation with *no* restriction imposed on how images should be represented, while requiring only that the representations are “close” to each other when the corresponding images are visually similar. The proposed algorithm is validated extensively using real-world datasets.

1. Introduction

With a growing demand for autonomous robots in a range of applications, such as search and rescue [42, 8], and space and underwater exploration [7], it is essential for the robots to be able to navigate accurately for an extended period of time in order to accomplish the assigned tasks. To this end, the ability to detect revisits (i.e., *loop closure* or place recognition) becomes necessary, since it allows the robots to bound the errors and uncertainty in the estimates of their positions and orientations (poses). In this work, we particularly focus on

¹Corresponding author, email: {yasir.latif@adelaide.edu.au}

loop closure during visual navigation, i.e., given a camera stream we aim to efficiently determine whether the robot has previously seen the current place or not.

Even though the problem of loop closure has been extensively studied in the visual-SLAM literature (e.g., see [30, 13, 21]), a vast majority of existing algorithms typically require the *offline* training of visual words (dictionary) from *a priori* images that are acquired previously in visually similar environments. Clearly, this is not always the case when a robot operates in an unknown, drastically different environment. In general, it is difficult to reliably find loops in (visual) appearance space. One particular challenge is the perceptual aliasing – that is, while images may be similar in appearance, they might be coming from different places. To mitigate this issue, both temporal (i.e., loops will only be considered closed if there are other loops closed nearby) and geometric constraints (i.e., if a loop has to be considered closed, a valid transformation must exist between the matched images) can be employed [21]. It is important to point out that the approach of [21] decides on the quality of a match *locally* – If the match with the highest score (in some distance measure) is away from the second highest, it is considered a valid candidate. However, the local information may lead to incorrect loop-closure decisions because both temporal and geometric conditions can easily fail in highly self-similar environments such as corridors in a hotel.

To address the aforementioned issues, in this paper we introduce a *general, online* loop-closure approach for vision-based robot navigation. In particular, by realizing that loops typically occur intermittently in a navigation scenario, we, for the first time ever, formulate loop-closure detection as a sparse ℓ_1 -minimization problem that is convex. This is opposed to the current methods that cast loop closure detection as an image retrieval problem [21, 13]. By leveraging the fast convex optimization techniques, we subsequently solve the problem efficiently and achieve real-time frame-rate generation of loop-closure hypotheses. Furthermore, the proposed formulation enjoys *flexible* representations and can produce loop-closure hypotheses regardless of what the extracted features represent – that is, any discriminative information, such as descriptors, Bag of Words (BoW), or even whole images, can be used for detecting loops. Lastly, we shall stress that our proposed approach declares a loop that is valid only when it is *globally unique*, which ensures that if perceptual aliasing is being caused by more than one previous image, *no* loop closure will be declared. Although this is conservative in some cases, since a false loop closing can be catastrophic while missing a loop closure generally is not, ensuring such global uniqueness is necessary and important, in particular, in highly self-similar environments.

The rest of the paper is organized as follows: After reviewing the related work, we formulate loop-closure detection as a sparse ℓ_1 -minimization problem in Section 3. In Section 4 we present in detail the application

of this formulation to visual navigation, which is validated via the real-world experiments in Section 5. Finally, Section 6 concludes this work as well as outlines the possible directions for future research.

2. Related Work

The problem of loop-closure detection has been extensively studied in the SLAM literature and many different solutions have been proposed over the years (e.g., see [24, 30] and references therein). In what follows, we briefly overview the work that closely relates to the proposed approach.

In particular, the FAB-MAP [13] is a probabilistic appearance-based approach using visual BoW for place recognition, and was shown to work robustly over trajectories up to 1000 km. Similarly, the Binary-BoW (BBoW)-based method [21] detects the FAST keypoints [38] and employs a variation of the BRIEF descriptors [6] to construct the BoW. A verification step is further enforced to geometrically check the features extracted from the matched images. It should be pointed out that both methods [13, 21] are based on the similar ideas of text-retrieval [34, 40]: These methods learn the BoW dictionaries beforehand, which are used later for detecting loop closures when the robots actually operates in the field. This restricts the expressive power of the dictionary in cases where it has to operate in environments drastically different from where the dictionary was constructed. In contrast, the proposed approach builds the dictionary *online* as the robot explores an unknown environment, while at the same time efficiently detecting loops (if any). Moreover, rather than solely relying on the descriptors-based BoW, our method is flexible and can utilize *all* pixel information to discriminate places even in presence of dynamic objects (encoded as sparse errors), any descriptor that can represent similar places, or any combination of such descriptors.

Some recent work has focused on loop closure under extreme changes in the environment such as different weather and/or lighting conditions at different times of the day. For example, Milford and Wyeth [33] proposed the SeqSLAM that is able to localize with drastic lighting and weather changes by matching sequences of images with each other as opposed to single images. Churchill and Newman [12] introduced the experience-based maps that learn the different appearances of the same place as it gradually changes in order to perform long-term localization. Building upon [12], Paul and Newman [36] also discovered new images to attain better localization. In addition, Lee et al. [28, 29] have explored geometric features such as lines for the task of loop closure detection in both indoor and outdoor scenarios. Note that if the information invariant to such changes can be extracted as in [13, 21, 33, 12, 36, 28, 29], the proposed formulation can also be used to obtain loop-closure hypotheses. Essentially, in this work we focus on finding loop closures

given some discriminative descriptions such as descriptors and whole images, assuming *no* specific type of image representations.

More recently, with the rediscovery of efficient machine learning techniques, Convolutional Neural Networks (CNNs)[4, 27] have been exploited to address loop closure detection [44, 45]. These networks are multi-layered architectures that are typically trained on millions of images for tasks such as object detection and scene classification. The internal representations at each layer are learned from the data itself and therefore can be used as features to replace hand-crafted features. Based on this approach, Sünderhauf et al. [44] extract features from different layers in the network and identify the layers that are useful for view-point and illumination invariant place recognition. Moreover, in [45] landmarks are treated as objects by finding object proposals in the images and features are extracted for them using deep networks. These features then allow for view-point invariant place categorization by matching different objects from varied viewpoints. In these CNN-based place categorization techniques, the networks are used as feature extractors followed by some form of matching. In this paper, we show that these deep features can also be utilized in the proposed framework of loop-closure detection.

It should be noted that in our previous conference publication [26], we have preliminarily shown that the proposed loop-closing framework is general and can employ most hand-crafted features. Recently, Shakeri and Zhang [39] extended this sparse-optimization based framework to an incremental formulation allowing for the use of the previous solution of the sparse optimization to jump start the next one, while Zhang et al. [46] further extended it to a multi-step delayed detection of loops (instead of single-step detection as in our prior work [26]) in order to exploit the structured sparsity of the problem. In this paper, we present more detailed analysis and thorough performance evaluations, including new experiments using deep features and validations in challenging multiple-revisit scenarios, as well as new comparisons against the well-known nearest neighbour (NN) search.

3. Sparse Optimization for Loop Closure

In this section, we formulate loop-closure detection as a sparse optimization problem based on a sparse and redundant representation. Such representations have been widely used in computer vision for problems such as denoising [19], deblurring [18], and face recognition [11]. Similarly, Casafranca et al. [9, 10] formulated the back-end of graph SLAM as an ℓ_1 -minimization problem. However, *no* prior work has yet investigated this powerful technique for loop closure detection in robot navigation. The key idea of

this approach is to represent the problem *redundantly*, from which a *sparse* solution is sought for a given observation.

Suppose that we have the current image represented by a vector $\mathbf{b} \in \mathcal{R}^n$, which can be either the vectorized full raw image or descriptors extracted from the image. Assume that we also have a dictionary denoted by $\mathbf{B} = [\mathbf{b}_1 \cdots \mathbf{b}_m] \in \mathcal{R}^{n \times m}$, which consists of m basis vectors of the same type as \mathbf{b} . Thus, solving the linear system $\mathbf{B}\mathbf{x} = \mathbf{b}$ yields the representation of \mathbf{b} in the base \mathbf{B} in the form of the vector $\mathbf{x} \in \mathcal{R}^m$. Elements of \mathbf{x} indicate which basis vectors, \mathbf{b}_i , best explain \mathbf{b} and how much the corresponding contributions are. A zero contribution ($x_i = 0$) simply implies that the corresponding basis vector \mathbf{b}_i is irrelevant to \mathbf{b} . One trivial example of a dictionary is the $n \times n$ identity matrix, $\mathbf{B} = \mathbf{I}_n$, which gives us the same representation, i.e., $\mathbf{I}_n \mathbf{x} = \mathbf{b} \Rightarrow \mathbf{x} = \mathbf{b}$. It is important to note that we have made *no* assumption about what the dictionary contains, and in general, any arbitrary bases including random matrices or wavelets can be used as a dictionary.

We know that a general vector \mathbf{b} can be represented by a basis matrix \mathbf{B} if and only if it belongs to the range space of \mathbf{B} , i.e., $\exists \mathbf{x} \neq \mathbf{0}$, s.t. $\mathbf{B}\mathbf{x} = \mathbf{b}$. Carefully choosing these bases may result in a sparse representation, i.e., \mathbf{x} is sparse. Very often this is the case in practice, because the signal is naturally sparse when represented in a certain, often overcomplete, basis [19]. For instance, when representing an image using the wavelet basis, there are only a few coefficients that are nonzero. Note also that a vector may not be representable by the bases, for example, if the basis matrix (dictionary) is rank-deficient and the vector is in the right nullspace of the matrix. To exclude such singular cases, in this work, we assume that the image vector \mathbf{b} is always representable by the basis matrix which is of full row rank (i.e., $\text{rank}(\mathbf{B}) = n$). Moreover, we allow the bases to be redundant, that is, we may have more (not necessarily orthogonal) basis vectors than the dimension of the image vector (i.e., $m > n$). Note that this assumption can be satisfied by carefully designing the dictionary (see Section 4). In general, a redundant dictionary leads to the sparse representation of the current image, which is what we seek and describes the sparse nature of the loop-closure events (i.e., occurring sparsely).

Consider that we have $m > n$ basis vectors, then $\mathbf{B}\mathbf{x} = \mathbf{b}$ becomes an under-determined linear system and has infinitely many solutions. Therefore, we have to regularize it in order to attain a unique solution by specifying a desired criterion that the solution should satisfy. Typically, this regularization takes the form of looking for a solution, \mathbf{x}^* , that leads to the minimum reconstruction error in the ℓ_2 -norm sense, which

corresponds to the least-squares formulation:

$$\min_{\mathbf{x}} \|\mathbf{B}\mathbf{x} - \mathbf{b}\|_2^2 \Rightarrow \mathbf{x}^* = \mathbf{B}^T(\mathbf{B}\mathbf{B}^T)^{-1}\mathbf{b} \quad (1)$$

Note that ℓ_2 -norm is widely used in practice in part because of the closed-form unique solution, while leading to a *dense* representation, i.e., almost all of the elements of \mathbf{x}^* are non-zero and thus all the basis vectors are involved in representing the current image vector. This goes against our prior knowledge of loop closures occurring sparsely. Theoretically, the least-squares solution can lie very far from the sparse solution for an underdetermined system [16], which motivates the ensuing sparse formulation.

Due to the fact that loop-closure events often occur sparsely, we instead aim to find the *sparsest* possible solution under the condition that it best explains the current image. Intuitively, by assuming that the basis dictionary consists of all the previous observed images and thus is redundant, we are looking for the smallest possible subset of previous images that can best explain the current image. The smallest such subset would contain just a single image which is “closest” to the current image (in appearance or descriptor space) under the assumption that there exists a unique image from the past which matches the current image. To that end, we employ the ℓ_0 -norm to quantify the sparsity of a vector, i.e., $\|\mathbf{x}\|_0 = \text{Card}(\mathbf{x} : \forall i, x_i \neq 0)$, the total number of non-zero elements in \mathbf{x} . Note that a vector with d non-zero elements is called d -sparse. Thus, the problem of loop closure can be formulated as follows:

$$\min_{\mathbf{x}} \|\mathbf{x}\|_0 \quad \text{subject to} \quad \mathbf{B}\mathbf{x} = \mathbf{b} \quad (2)$$

The above problem is a combinatorial optimization problem which in general is NP-hard [1], because all of the possible d -sparse vectors have to be enumerated to check whether they fulfill the constraint. To address this computational-intractability issue, we relax the ℓ_0 -norm in (2) to ℓ_1 -norm, which is defined as the summation of absolute values of the elements of \mathbf{x} , $\|\mathbf{x}\|_1 = \sum_{i=1}^n |x_i|$, since it is known that ℓ_1 -norm is the closest convex approximation to ℓ_0 -norm and also results in a sparse solution [15], i.e.,

$$\min_{\mathbf{x}} \|\mathbf{x}\|_1 \quad \text{subject to} \quad \mathbf{B}\mathbf{x} = \mathbf{b} \quad (3)$$

The problem (3) assumes the perfect reconstruction without noise, which clearly is not the case in practice. Hence, we introduce a sparse noise (error) term along with the basis vectors to explain the current image and reformulate (3) as follows:

$$\min_{\mathbf{x}, \mathbf{e}} \|\mathbf{x}\|_1 + \|\mathbf{e}\|_1 \quad \text{subject to} \quad \mathbf{B}\mathbf{x} + \mathbf{e} = \mathbf{b} \quad (4)$$

$$\Rightarrow \min_{\boldsymbol{\alpha}} \|\boldsymbol{\alpha}\|_1 \quad \text{subject to} \quad \mathbf{D}\boldsymbol{\alpha} = \mathbf{b} \quad (5)$$

where $\mathbf{D} := \begin{bmatrix} \mathbf{I}_n & \mathbf{B} \end{bmatrix}$ and $\boldsymbol{\alpha} := \begin{bmatrix} \mathbf{e} \\ \mathbf{x} \end{bmatrix}$. Note that we have normalized the basis vectors when building the dictionary \mathbf{D} , and thus \mathbf{I}_n can be considered as the noise bases along each of the n directions of the data space, and \mathbf{e} becomes an indication variable for which noise components dominate the reconstruction error. This allows us to normalize \mathbf{x} and \mathbf{e} together when computing contributions of data and noise bases (see Section 4.1). We stress that this new formulation of loop closure (5) takes advantage of the fact that ℓ_1 -norm automatically promotes sparsity, as opposed to the more commonly used ℓ_2 -based least-squares formulation [3]. In solving (5) for a minimum ℓ_1 -norm solution, we are in effect seeking an explanation of the current image with the fewest basis vectors from the redundant dictionary. This problem is also known as atomic decomposition [19], since \mathbf{b} is decomposed into its constituent atoms in the dictionary.

4. Closing Loops via ℓ_1 -Minimization

We have formulated loop closure as a sparse convex ℓ_1 -minimization problem (5) in the preceding section. We now present in detail how this novel formulation can be utilized in vision-based robot navigation. In what follows, we first explain how a dictionary can be constructed *incrementally online*, and then how such a dictionary can be used at *each time step* to generate loop-closure hypotheses.

4.1. Building Dictionary

The first step in the proposed process of detecting loops is to build a set of basis vectors that make up the dictionary. Unlike the state-of-the-art loop-closure detection methods (e.g., [21]), the proposed approach does *not* learn the dictionary *offline* before the start of the experiment. Instead, the dictionary is built exclusively for the current experiment, as the robot moves and collects images – that is, *incrementally online* as images arrive.

As a new image becomes available, a mapping function, $\mathbf{f} : \mathcal{R}^{(r,c)} \rightarrow \mathcal{R}^n$, transforms the image of resolution $r \times c$ to a unit vector of dimension n . Due to the flexibility of representation enjoyed by our proposed approach, this function is general and can be either a whole image or descriptors such as HOG [14] and GIST [35] computed over the image. That is, the basis vectors can represent any information that helps distinguish between two images. The proposed method can be considered as data association in a high-dimensional space carried out by (approximately) reconstructing a given vector from a subset of unit vectors in that space. As such, this approach is agnostic to what these vectors physically represent. For this reason, versatility of representation is inherent to our algorithm, allowing representations ranging from

whole images to descriptors, BoW, or even mean and variance normalized images over time for matching sequences across different times of day or changing weather conditions. Also, since we use the ℓ_2 -norm of the error (i.e., Euclidean distance) to measure how good the reconstruction is, any descriptor whose distance between two vectors is measured in term of ℓ_2 -norm, can be naturally incorporated in the proposed approach.

In order to ensure full row rank of the dictionary matrix \mathbf{D} , we initialize the dictionary with an identity matrix \mathbf{I}_n , which also accounts for the bases of the noise e [see (5)]. When the first image denoted by i_1 arrives, $\mathbf{b}_1 = \mathbf{f}(i_1)$ is added to the dictionary. In general, updating the dictionary at the i -th time step is simply appending $\mathbf{b}_i = \mathbf{f}(i_i)$ to the end of the current dictionary². However, before augmenting the dictionary, we need to determine whether or not there are some previous images that explain the current one, i.e., we need to detect any loop that can be closed based on the current image.

4.2. Solving ℓ_1 -Minimization

Once the dictionary \mathbf{D} is available and when an image arrives at every time step, we are now ready to solve the convex, sparse ℓ_1 -minimization problem (5) in order to find (if any) loop closures. While various approaches such as the primal-dual method are available for solving a convex optimization problem [5], we here leverage the homotopy approach because of its efficiency [31, 17], which is specifically designed to take advantage of the properties of ℓ_1 -minimization.

In particular, relaxing the equality constraint in (5) yields the following *constrained* minimization:

$$\min_{\boldsymbol{\alpha}} \|\boldsymbol{\alpha}\|_1 \quad \text{subject to} \quad \|\mathbf{D}\boldsymbol{\alpha} - \mathbf{b}\|_2 \leq \epsilon \quad (6)$$

where $\epsilon > 0$ is a pre-determined noise level. This is termed the basis pursuit denoising problem in compressive sensing [15]. An equivalent variant of (6) is the following *unconstrained* minimization problem that is actually solved by the homotopy approach:

$$\min_{\boldsymbol{\alpha}} \lambda \|\boldsymbol{\alpha}\|_1 + \frac{1}{2} \|\mathbf{D}\boldsymbol{\alpha} - \mathbf{b}\|_2^2 \quad (7)$$

where λ is a scalar weighting parameter. To solve (7), the homotopy method uses the fact that the objective function undergoes a homotopy continuation from the ℓ_2 cost (the second term) to the ℓ_1 cost (the first term) as λ increases from zero to one [17]. The computational complexity of this approach is $O(dn^2 + dnm)$ for

² Although this simple augmentation would make the dictionary grow unbounded, more sophisticated update policies (e.g., replacing or merging basis vectors for the same locations) can be designed in order to control the size of the dictionary when a robot repeatedly operates in the same environment.

Algorithm 1 Closing Loops via ℓ_1 -Minimization

Input: Dictionary \mathbf{D}_{i-1} , Current image \mathbf{i}_i , Threshold τ , Weight λ , Ignoring-time window t_g

Output: Loop-closure hypotheses \mathbf{H} , Updated dictionary \mathbf{D}_i

- 1: $\mathbf{b}_i := \mathbf{f}(\mathbf{i}_i)$
 - 2: *Hypothesis generation:*
 - 3: Solve $\min_{\boldsymbol{\alpha}_i} \lambda \|\boldsymbol{\alpha}_i\|_1 + \frac{1}{2} \|\mathbf{D}_{i-1}\boldsymbol{\alpha}_i - \mathbf{b}_i\|_2$ using the homotopy approach (see Section 4.2)
 - 4: Normalize $\hat{\boldsymbol{\alpha}}_i := \frac{\boldsymbol{\alpha}_i}{\|\boldsymbol{\alpha}_i\|_2}$
 - 5: Find hypotheses $\mathbf{H} := \{j \mid \hat{\alpha}_{i,j} > \tau, \|i - j\|_1 > t_g\}$
 - 6: *Dictionary update:*
 - 7: $\mathbf{D}_i := \begin{bmatrix} \mathbf{D}_{i-1} & \mathbf{b}_i \end{bmatrix}$
-

recovering a d -sparse signal in d steps using an $n \times m$ dictionary, although in the worst case when recovering a non-sparse solution in a high-dimensional observational space and large number of basis vectors, it can perform as worse as $O(m^3)$, which fortunately is not the case in this work.

The above homotopy solver is employed to determine loop closure for the i -th image represented by \mathbf{i}_i , by solving (7) for $\mathbf{f}(\mathbf{i}_i)$ using the up-to-date dictionary $\mathbf{D}_{i-1} = \begin{bmatrix} \mathbf{I}_n & \mathbf{f}(\mathbf{i}_1) & \dots & \mathbf{f}(\mathbf{i}_{i-1}) \end{bmatrix}$.³ The solution $\boldsymbol{\alpha}_i = \begin{bmatrix} \alpha_{i,1} & \dots & \alpha_{i,n+i-1} \end{bmatrix}^T$ at the i -th time step contains the contribution of all previous bases in constructing the current image. To find a unique image to close a loop with, we are interested in which basis vector has the greatest relative contribution, which can be found by calculating the unit vector $\hat{\boldsymbol{\alpha}}_i = \boldsymbol{\alpha}_i / \|\boldsymbol{\alpha}_i\|_2$. Any entry greater than a predefined threshold, τ , is considered a loop-closure candidate. In addition, due to the fact that in a visual navigation scenario, the neighbouring images are typically overlapped with the current image and thus have great “spurious” contributions, we explicitly ignore a time window, t_g , around the current image, during which loop-closure decisions are not taken. This is a design parameter and can be chosen based on the camera frequency (fps) and robot motion. Once the decision is made, the dictionary is updated by appending $\mathbf{f}(\mathbf{i}_i)$ to it, i.e., $\mathbf{D}_i = \begin{bmatrix} \mathbf{D}_{i-1} & \mathbf{f}(\mathbf{i}_i) \end{bmatrix}$. The main steps of this process are summarized in Algorithm 1.

³The subscript $i - 1$ is hereafter used to denote the time index, thus revealing the online incremental process of the proposed approach.



Figure 1: Sample images from the New College dataset: Query images (top) and the corresponding match images (bottom). The images are down-sampled to 8×6 pixels. Note that in spite of dynamic changes and motion blurs occurring in these images which deteriorate the loop-closure problem, the proposed approach still provides reliable results.

4.3. Remarks

4.3.1. Global uniqueness

It is important to note that the solution to (7), by construction, is guaranteed to be sparse. In the ideal case of no perceptual aliasing, the solution is expected to be 1-sparse, because *ideally* there exists only one image in the dictionary that matches the current image when a revisit occurs. In the case of exploration where there is no actual loop-closure match in the dictionary, the current image is best explained by the last observed and the solution hence is still 1-sparse, which however will not generate a valid loop-closure detection because of the temporal constraint t_g enforced in our implementation. Note that if there are significant differences such as illumination or dynamic objects, the solution may no longer be 1-sparse (see Section 5.7).

In a general case where $k > 1$ images that have been previously observed and that are visually similar to the current image, a naive thresholding based method – which simply compares the current image to each of the previous ones based on some similarity measure – would likely produce k loop-closure hypotheses corresponding to the k images in the dictionary. It is very important to note that such an approach independently calculates the contribution of each previous image, *without* taking into account the effects of other images or data noise, despite the fact that due to noise they may be correlated and thus is *suboptimal*. In contrast, the proposed ℓ_1 -minimization-based approach simultaneously computes the optimal contribution of all the previous images and noise by finding the global optimal solution $\hat{\alpha}_i$ of the convex problem (7), and

guarantees the unique hypothesis by selecting the j -th image with the greatest $\hat{\alpha}_{i,j}$.

In the case of multiple revisits to the same location, the proposed approach, as presented here, is *conservative* (i.e, only one, but the best one, revisit would be selected). Including the corresponding images from earlier visits in the dictionary would lead to a non-unique solution, when the same location is revisited again. However, the proposed method can be easily extended to detect loops on multiple revisits. Instead of considering the contribution of all the previous basis separately, if a loop exists between previous locations k and l , we consider their joint contribution ($\hat{\alpha}_{i,k} + \hat{\alpha}_{i,l}$) when making the decision. This ensures that even though these places are not individually unique enough to explain the current image, together (and since they are visually similar as we already have a loop closure between them), they best explain the current observation, allowing us to detect loop closures in case of multiple revisits.

4.3.2. Flexible basis representation

We stress that the dictionary representation used by the proposed approach is general and flexible. Although we have focused on the simplest basis representation using the down-sampled whole images (see Section 5), this does not restrict our method only to work with this representation. In fact, any discriminative feature that can be extracted from the image (e.g., GIST, HOG, etc.) can be used as dictionary bases for finding loops, thus permitting the desired properties such as view and illumination invariance. To show that, particular experiments have been performed in Section 5, using different types of bases and their combinations. Moreover, it is not limited to a single representation at a time. If we have k descriptors $f_i : \mathcal{R}^{(r,c)} \rightarrow \mathcal{R}^{k_i}$, a multi-modal descriptor can be easily formed by stacking them up in a vector in \mathcal{R}^K ($K = \sum_{i=1}^k k_i$). This idea has recently been exploited in [46]. Therefore, our proposed method can be considered as a *generalized* loop-closing approach that can use any basis vectors as long as a metric exists to provide the distance between them.

4.3.3. Robustness

It is interesting to point out that sparse ℓ_1 -minimization inherently is robust to *data noise*, which is widely appreciated in computer vision (e.g., see [11]). In particular, the sparse noise (error) term in (5) can account for the presence of dynamic changes or motion blurs. For example, in Fig. 1 the dominant background basis explains most of the image, while the dynamic elements (which have not been observed before) can be represented by the sparse noise, and Fig. 2 shows that the proposed approach robustly finds these loops. Such robust performance becomes necessary particularly for long-term mapping where the environment often gradually changes over time and thus reliable loop closure in presence of such changes is essential.

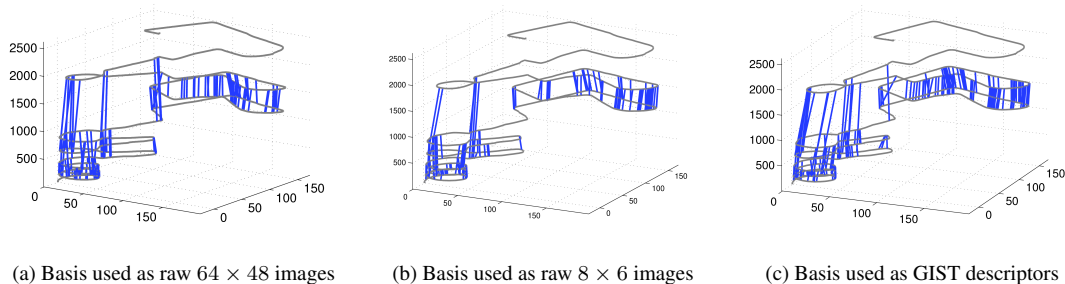


Figure 2: Loop closures detected by the proposed approach using two different bases for the New College dataset. In these plots, visual odometry provided with the dataset is shown in gray while the loop closures are shown in blue. The z -axis represents time (in seconds) and the x - and y -axes represent horizontal position (in meters).

As a final remark, the proposed ℓ_1 -minimization-based loop-closure algorithm is also robust to *information loss*, which is closely related to the question raised by Milford [32]: How much information is needed to successfully close loops? In this work, we have empirically investigated this problem by down-sampling the raw images (which are used as the bases of the dictionary) without any undistortion and then evaluating the performance of the proposed approach under such an adverse circumstance. As shown in Section 5, truly small raw images, even with size as low as 48 pixels, can be used to reliably identify loops, which agrees with the findings of [32].

5. Experimental Results

To validate the proposed ℓ_1 -minimization-based loop-closure algorithm, we perform a set of real-world experiments on the publicly-available datasets. In particular, a qualitative test is conducted on the New College dataset [41], where we examine the different types of bases (raw images and descriptors) in order to show the flexibility of basis representation of our approach as well as the robustness to dynamics in the scene. Subsequently, we evaluate the proposed method on the RAWSEEDS dataset [37] and focus on the effects of the design parameters used in the algorithm. Finally, we perform experiments on the KITTI Visual Odometry Benchmark [22], by highlighting the ability of the proposed approach to use different types of deeply learned features as representations, as well as the superior performance against a nearest neighbour (NN)-based approach.

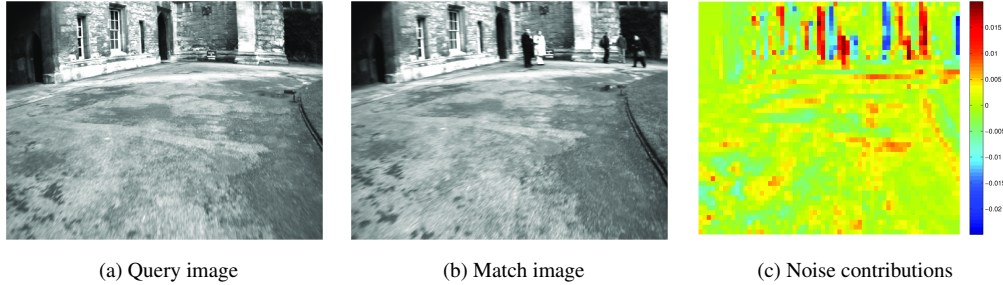


Figure 3: A typical dynamic scenario in the New College dataset: When querying a current image to the dictionary that uses 64×48 raw images as its bases, the proposed approach robustly finds the correct match – which however is contaminated with moving people – by modelling the dynamics as noise.

5.1. New College: Different Types of Basis

The New College dataset [41] provides stereo images at 20 Hz along a 2.2 km trajectory, while in this test we only use every 20th frame giving an effective frame rate of 1 Hz and in total 2624 images. Each image originally has a resolution of 512×384 , but here is down-sampled to either 64×48 or 8×6 pixels. We show below that even under such adverse circumstance, the proposed approach can reliably find the loops. The image is scaled so that its gray levels are between zero and one, and then is vectorized and normalized as a unit column vector. For the results presented in this test, we use the threshold $\tau = 0.99$ and the weighting parameter $\lambda = 0.5$. Due to the fact that neighbouring images typically are similar to the current one and thus generate false loop closures, we ignore the hypotheses within a certain time window from the current image and set $t_g = 10$ sec, which effectively excludes the spurious loops when reasoning about possible closures. Note that t_g can be chosen according to speed of the robot as well as the frame-rate at which the loop closing algorithm is working. We also eliminate random matches by enforcing a temporal consistency check, requiring at least one more loop closure within a time window from the current match. We ran all the experiments in Matlab on a Laptop with Core-i5 CPU of 2.5GHz and 16 GB RAM, and use the homotopy-based method [2] for solving the optimization problem (7).

The qualitative results are shown in Fig. 2 where we have used *three* different bases, i.e, down-sampled 64×48 and 8×6 raw images, and GIST descriptors. In these plots, the odometry-based trajectory provided by the dataset is superimposed by the loop closures detected by the proposed approach, which are shown as vertical lines connecting two locations where a loop is found. All the lines parallel to the z -axis represent

loop closures that connect the same places at different times. Any false loops would appear as non-vertical lines, and clearly do not appear in Fig. 2, which validates the effectiveness of the proposed method in finding correct loops. These results clearly show the flexibility of bases representation of the proposed method. In particular, instead of using the different down-sampled raw images as bases, our approach can use the GIST descriptors, $\mathbf{GIST}(\mathbf{b}) \in \mathcal{R}^{512}$, which are computed over the whole image, and is able to detect the same loop closures as with the raw images.

An interesting way of visualizing the locations where loop closures occur is to examine the sparsity pattern of the solution matrix, which is obtained by stacking all the solutions, $\hat{\alpha}_i$, for all the queried images in a matrix. Fig. 4 shows such a matrix that contains non-zero values in each column corresponding to the elements greater than the threshold τ . In the case of no loop closure, each image can be best explained by its immediate neighbour in the past, which gives rise to non-zeros along the main diagonal. Most importantly, the off-diagonal non-zeros indicate the locations where loops are closed. It is interesting to see that there are a few sequences of loop closures appearing as off-diagonal lines in Fig. 4. This is due to the fact that the first three runs in the circular area at the beginning of the dataset, correspond to the three off-diagonal lines in the top-left of the matrix; while a sequence of loop closures detected in the lower part of New College, correspond to the longest line parallel to the main diagonal.

It is important to note that although both dynamic changes and motion blurs occur in the images, the proposed approach is able to reliably identify the loops (e.g., see Fig. 1), which is attributed to the sparse error used in the ℓ_1 -minimization [see (5)]. To further validate this robustness to dynamics, Fig. 3 shows a typical scenario in the New College where we query a current image with no dynamics to the dictionary that uses 64×48 down-sampled raw images as its bases, and the correct match is robustly found, which however contains moving people. Interestingly, the dominant noise contributions (blue) as shown in Fig. 3(c), mainly correspond to the locations where the people appear in the match image. This implies that the sparse error in (5) correctly models the dynamic changes.

5.2. RAWSEEDS: Effects of Design Parameters

To further test the proposed algorithm, we use the Bicocca 25b dataset from the RAWSEEDS project [37]. The dataset provides the laser and stereo images for a trajectory of 774 m. We use the left image from the stereo pair sampled at 5 Hz, resulting in a total of 8358 images. Note that we do *not* perform any undistortion and work directly with the raw images coming from the camera. In this test, we focus on studying the effects of the most important parameters used in the proposed approach, and evaluate the

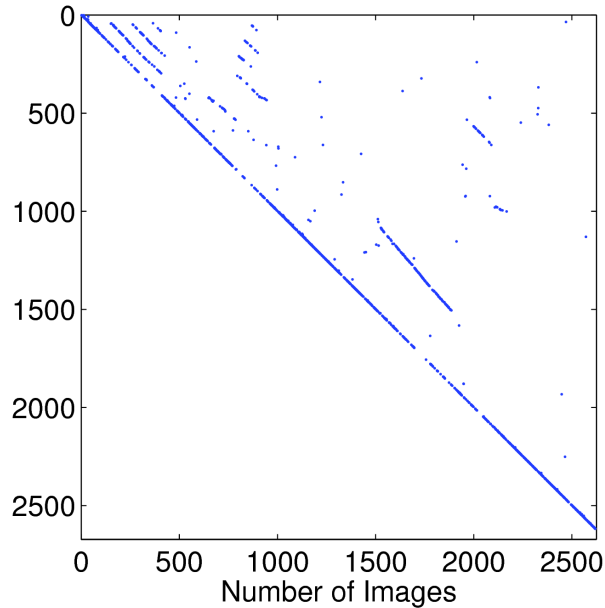


Figure 4: Sparsity pattern induced by solving (7) for *all* the images in the New College dataset. The i -th column corresponds to the solution for the i -th image, and the non-zeros are the values in each column that are greater than $\tau = 0.99$. Note that the main diagonal occurs due to the current image being best explained by its neighboring image, while the off-diagonal non-zero elements indicate the loop closures.

performance based on precision and recall. Specifically, precision is the ratio of correctly detected loop closures over all the detections. Thus, ideally we would like our algorithm to work at full precision. On the other hand, recall is the percentage of correct loop closures that have been detected over all possible correct detections. A high recall implies that we are able to recover most of the loop closures.

5.2.1. Threshold τ and weight λ

We first examine the acceptance threshold τ , whose valid values range from 0.5 to 1. This parameter can be thought of as the similarity measure between the current image and the matched image in the dictionary. In order to study the effect of this parameter on the precision and recall, we vary the parameter for a fixed image of 20×15 pixels. Moreover, we are also interested in if and how the weighting parameter λ impacts the performance and thus vary this parameter as well.

The results are shown in Fig. 5. As expected, the general trend is that a stricter threshold (closer to 1)

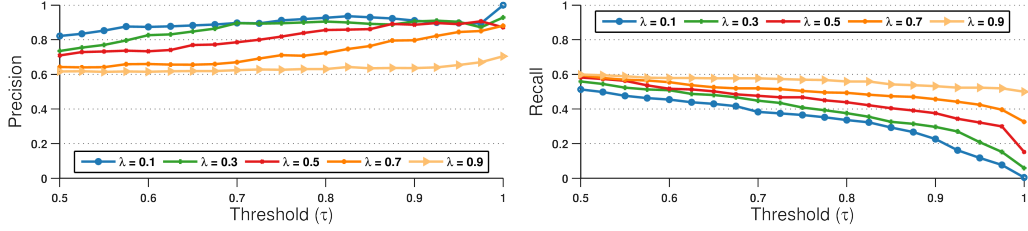


Figure 5: Precision and recall curves for the Bicocca dataset while using the 20×15 raw images.

leads to higher precision, and as a side effect, a lower recall. This is because as the threshold increases, we get fewer loop closing hypotheses but a larger proportion of them is correct. Note that this dataset is challenging due to the perceptual aliasing in many parts of the trajectory; the matched images are visually similar but considered as false positives since the robot is physically not in the same place.

Interestingly, Fig. 5 also shows that the smaller λ leads to the higher precision but the lower recall. This seems to counter the intuition that the sparser the solution of (7) (by using a larger λ), the higher fidelity of the loop-closure detection. However, it should be noted that this intuition motivates the proposed sparse formulation but does not guarantee that the optimal solution is sparsest (1-sparse) as discussed in Section 4.3.1, which heavily depends on the quality of the data at hand (e.g., signal-to-noise ratio, the similarity level of the revisiting images). It is important to note that there are two goals to reconcile in our sparse formulation (7): (i) the reconstruction error represented by the ℓ_2 term, and (ii) the sparsity level of the solution encoded in the ℓ_1 term. A smaller value of this parameter results in a better data-fitting solution of smaller reconstruction error, hence requiring the images to be as visually similar as possible but at the same time, lowering the contribution of the greatest basis vector.

5.2.2. Image size

Inspired by the recent work [32], we also examine the performance difference by varying image sizes and see if we can obtain meaningful results using small-size images. The original image size from the Bicocca dataset is 320×240 , and the first image size we consider is 80×60 which is a reduction of a quarter in each dimension. For each successive experiment, we half the size in each dimension, which results in images of size 40×30 , 20×15 , 10×8 , and finally 5×4 . The weighting parameter λ is fixed to be 0.5. Precision and recall curves are generated by varying the acceptance threshold τ are shown in Fig. 6.

It is clear from Fig. 6 that the curves are tightly coupled and undergo the same behaviour for each image size. Precision curves for the three largest image sizes overlap each other, showing that we can generate

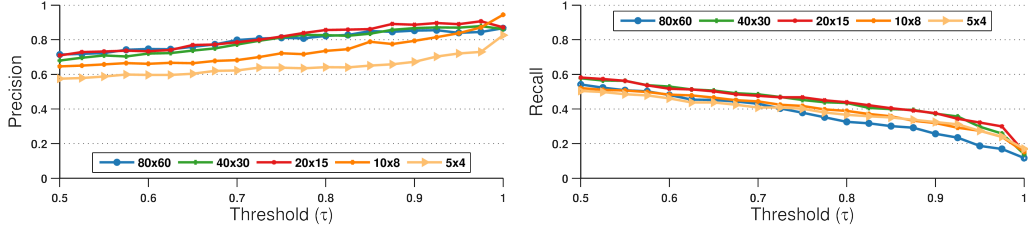


Figure 6: Precision and recall curves for the Bicocca dataset while fixing the weighting parameter $\lambda = 0.5$.

the same quality of loop closure hypotheses using any of the image sizes. These plots show a graceful degradation as the image size decreases. Considering that the image of size 10×8 is a factor of 960 times smaller than the original image, our method is able to distinguish places based on very little information, which agrees with the findings of [32].

5.2.3. Execution time

Since the proposed method solves an optimization problem in a high-dimensional space, it is important to see how long the method takes to come up with the loop-closing hypotheses. Despite that each image is an $r \times c$ vector for an image with r rows and c columns, and at the end of the experiment we have nearly 8500 images, the computation is very efficient thanks to the sparsity induced by the novel formulation. Most of our solutions are expected to be 1-sparse (i.e., we expect only one non-zero if the current image matches perfectly one of the basis vectors in the dictionary), and thus the homotopy-based solver performs efficiently as shown in Table 1. For the largest image size, the mean time is 117 ms with a maximum less than half a second. The proposed method works well on small images such as 20×15 , which take on average 3.7 ms. The runtime gradually grows as the number of basis vectors increases. The timing information given in Table. 1 shows that the current method can run fast enough for real time operation at above 5Hz for the largest image size considered.

Interestingly, we found $\lambda = 0.5$ is a good trade-off between precision/recall and computational cost. In general, a higher threshold τ would lead to fewer high-quality loop closures. This parameter can be designed based on the application in question. Similarly, images of size larger than 20×15 do not provide great improvement in terms of precision/recall. Thus, the choice of image size should take into account the complexity of the environment being modelled. In an environment (e.g., outdoors) where there is rich textural information, smaller images may be used. If the environment itself does not contain a lot of distinguishable features, larger images can be used in order to be able to differentiate between them.

Table 1: Execution time for different image sizes. Note that at the end, the dictionary has a size of feature dimension + 8358 (number of basis).

size (feature dimension)	min (ms)	mean (ms)	max (ms)	std (ms)
80×60 (4800)	45.762	116.45	417.290	43.229
40×30 (1200)	2.689	17.334	70.940	9.500
20×15 (300)	0.111	3.662	20.828	2.904
10×8 (80)	0.029	0.707	4.448	0.552
5×4 (20)	0.021	0.410	2.541	0.3163

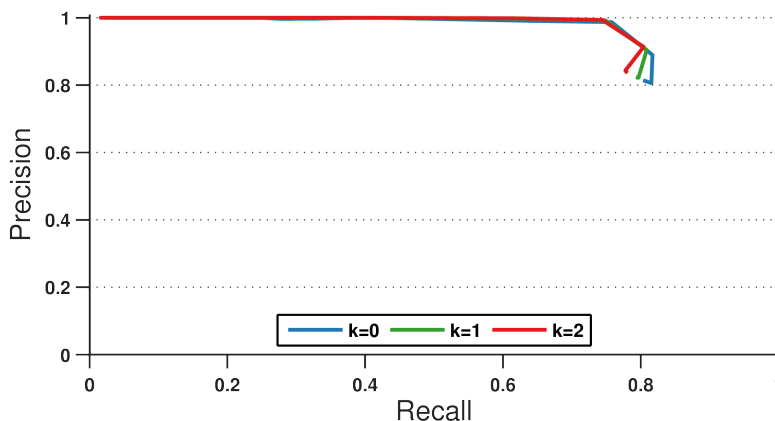


Figure 7: Precision and recall curves of DBoW [21] for the Bicocca dataset using the full-sized 320×240 images. In this plot, k denotes the values used for temporal consistency constraint.

5.3. Comparison to DBoW

In this section, we compare the performance of the proposed method against the state-of-the-art DBoW algorithm [21] on Bicocca 25b dataset. For the DBoW, we operate on the full-sized 320×240 images, using different temporal constraints ($k = 0, 1, 2$) along with geometric checks enabled. Its performance is controlled by a so-called confidence parameter $\alpha \in [0, 1]$. We sweep over the values of this parameter and compute the precision and recall for each α , which are shown in Fig. 7.

For the purpose of a fair comparison, we carry out the same geometric verification step in DBoW (Fig. 7) and in the proposed method (Fig. 8): feature extraction, matching and fitting a fundamental matrix between the matched features. If sufficient support is not found for the fundamental matrix, the proposed hypothesis

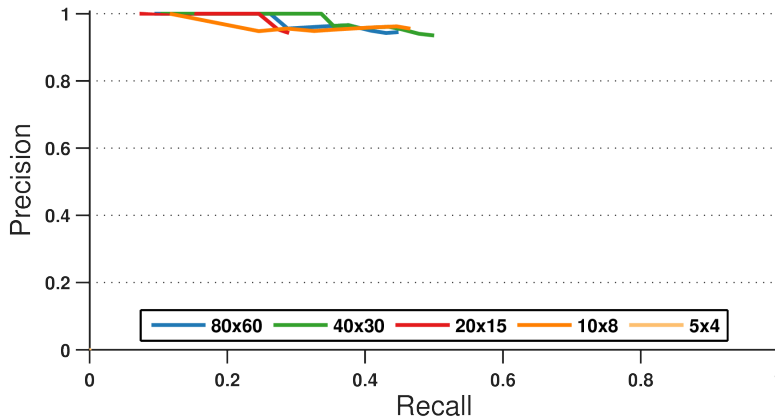


Figure 8: Precision and recall corresponding to Fig.6 with an additional geometric verification step, same as the one used in DBoW.

is rejected. This geometric verification is carried out on the full resolution images.

As seen from Figs. 7 and 8 , the best precision-recall curve of our method competes with that of the DBoW in terms of precision; moreover, the proposed algorithm is more conservative and operates with *lower* recalls. This low recall is a consequence of requiring the match to be globally unique in order to be considered a loop closure. Overall, the proposed approach achieves competitive trade-off between precision and recall.

5.4. Deep Features

Recently, many computer vision tasks have shown great boost in performance by using features from Convolutional Neural Networks (CNNs). Instead of using hand-crafted features, these networks learn features from data, which are a more “natural” representation for tasks such as image segmentation and object detection and are shown to outperform hand-crafted features such as SIFT and GIST, as shown in the PASCAL Visual Object Classes (VOC) Challenge [20]. To evaluate that these deep features can also be used in the proposed loop closing framework, we further test on the KITTI Visual Odometry benchmark [22]. The datasets consists of 21 trajectories recorded using multiple sensors, among which the ground truth is provided for 10 and only 6 contain at least one loop closure. The ground truth for the loop closures is used from the dataset presented in [25], where loop closures are calculated at 2Hz for the six trajectories with ground truth. In particular, we use the deep network presented in [23]. The network learns to represent a

given 64×64 image patch in \mathcal{R}^{256} for the task of patch matching. For the experiments presented here, we use this network as a feature extractor and employ different strategies.

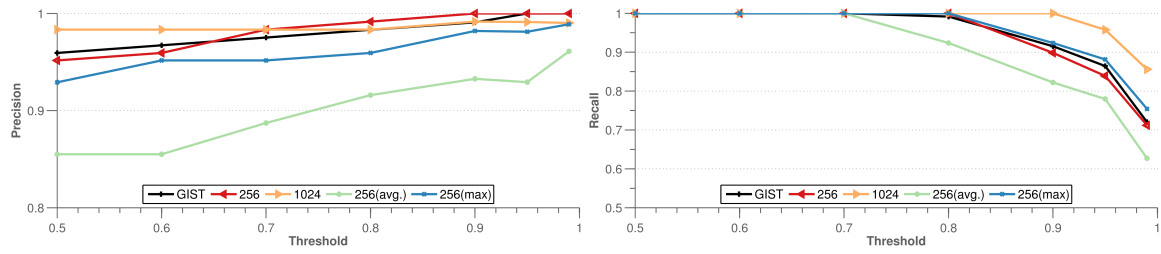
In the simplest case, we rescale the input image to 64×64 giving us a feature in \mathcal{R}^{256} . As an alternative strategy, we rescale the image to 128×128 resulting in four 64×64 input patches, leading to four vectors in \mathcal{R}^{256} as output. We either stack them to get a vector in \mathcal{R}^{1024} [1024], average them to get a vector in \mathcal{R}^{256} [256(avg.)], or take the element-wise maximum over them to get a vector in \mathcal{R}^{256} [256(max)], an operation termed max-pooling. We compare the performance of these various configurations derived from deep features with that of GIST for 4 sequences from the KITTI dataset. In these experiments, we vary the threshold (τ) to generate different loop closing proposals. The weighing parameter (λ) is set to 0.5. The results are presented in Fig. 9.

It can be seen that the learned features perform better than GIST in all the cases. The 1024 configuration is the most discriminative, leading to a smaller number of outliers and greater number of correct loop closures. Moreover, the performance of 256 is comparable and in most cases better than GIST, which is a 512 dimensional representation. This agrees with the insight that learned features have more expressive power compared to hand crafted ones. Averaging features from the deep network leads to them being less discriminative, leading to the worst performance in Fig. 9. It should be pointed out that the original image size for the images in the KITTI sequences is 1241×376 and the best performance is achieved with a very smaller 128×128 representation. Moreover, these experiments also highlight the fact that various representations can be used in the proposed framework for the task of loop closure detection.

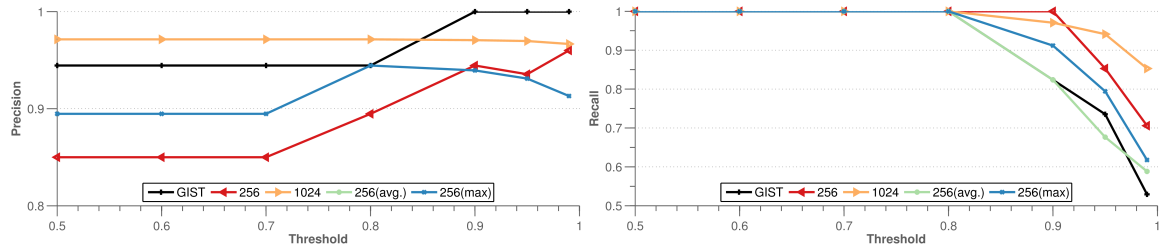
5.5. Multi-Modal Features

A desirable property of the proposed framework is that any unit vector can be used as a feature for carrying out loop closure detection. In the previous section, we showed experiments that used single-modal features including GIST and deep features for this purpose. However, we are not restricted to using just a single-modal feature. Two distinct features can be stacked to form a new multi-modal feature, that is, for two feature $\mathbf{f}_i \in \mathcal{R}^n$ and $\mathbf{f}_j \in \mathcal{R}^m$, a new feature $\mathbf{f}_{ij} \in \mathcal{R}^{(n+m)}$ can be obtained by $\mathbf{f}_{ij} = S(\mathbf{f}_i, \mathbf{f}_j) = [\mathbf{f}_i^T \ \mathbf{f}_j^T]^T$, followed by projection onto the unit sphere.

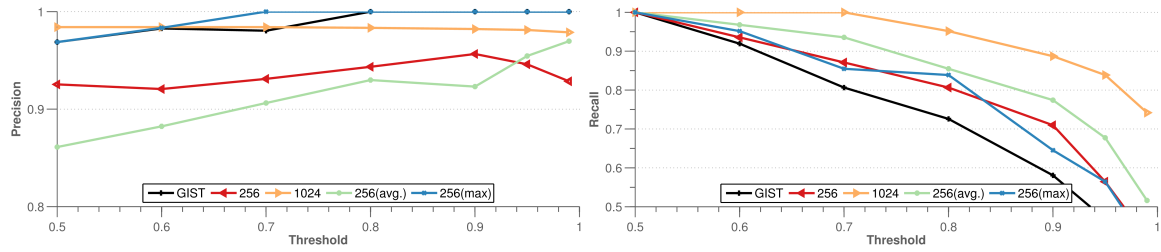
In order to investigate if this leads to better performance, we use combinations of the GIST and deep features described in Section. 5.4. For the three features: GIST, 256, and 1024, we explore the possible four combinations: **1)** S(GIST, 256), **2)** S(GIST, 1024), **3)** S(256, 1024), and **4)** S(GIST, 256, 1024). The results are presented in Fig. 10. Comparing it to Fig. 9, it can be seen that the performance is much better than the



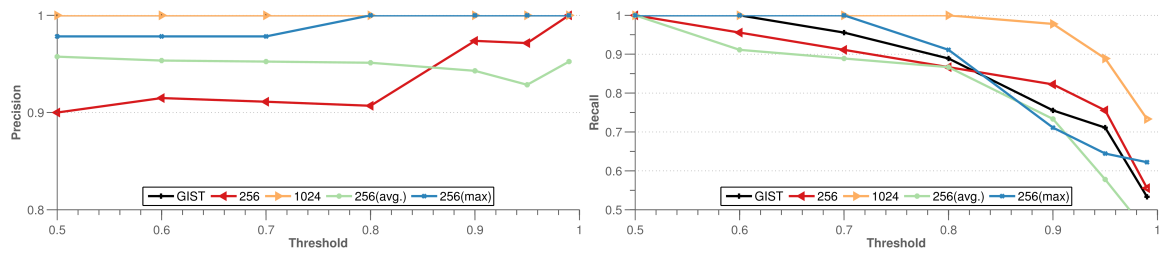
(a) Sequence 00



(b) Sequence 02



(c) Sequence 05



(d) Sequence 06

Figure 9: Precision and recall statistics of the proposed loop closing approach using deep features on the KITTI visual odometry benchmark. Please note that the Y-axis for the Precision starts at 0.8.

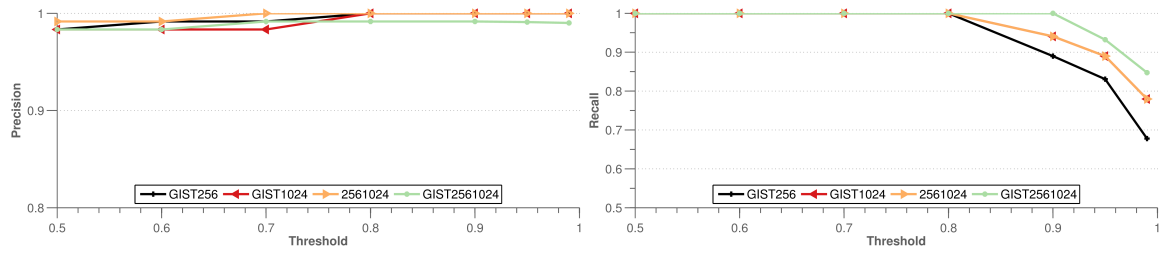
single features case, the precision is higher with a comparable recall.

The multi-modal features are more discriminative and can be thought to match images over the intersection of both the descriptor spaces, leading to a better precision. This, however, is achieved at the cost of an increased size of the final stacked descriptor. The largest size considered here is that of $S(\text{GIST}, 256, 1024)$ which is 1792. However, this is still feasible for runtime operation (see Table 1). This expressive power of the stacked features places images far away from each other in the new combined descriptor space, allowing sparser solutions and thus leading to a better recall as well.

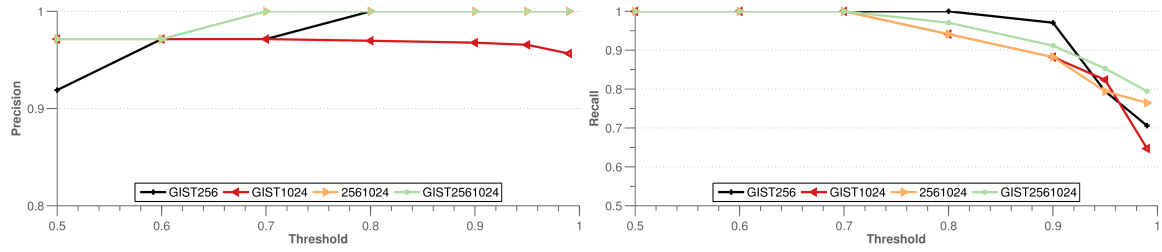
5.6. Repeated Visits

As highlighted in Section 4.3.1, the method declares loop closures that are globally unique. This may lead to missed loops in the worst case, that is, when either two images or the descriptors extracted from them are exactly the same. This is the worst case because in every other case, there would exist a single or a set of images that are able to reconstruct the image. Only in the case of the exact same basis vectors, multiple solution with the same value for (7) exist. In order to show how the proposed method behaves in the worst case, we take a batch of 100 images from the New College dataset and present the batch 60 times to the loop closing method. This simulates the situation of 60 repeated visit to the same place leading to the generation of the exact same images. Each image is described with a GIST descriptor of length 512. We use the proposed framework to solve for loop closures and look at the sparse solution $[\alpha_i$ in (7)] for each of the images presented to the method. We stack these α_i as column vectors and the results are shown in Fig. 11.

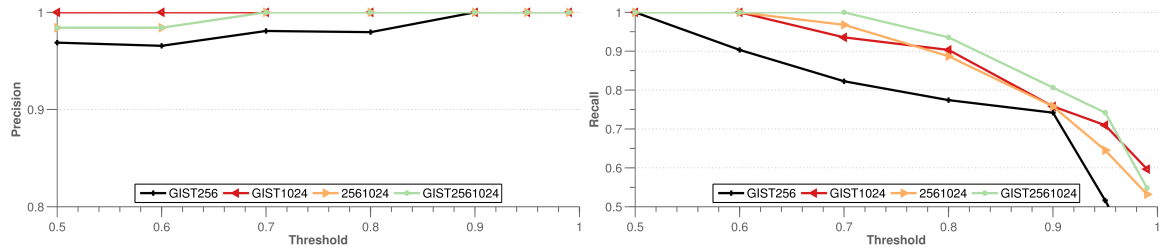
The method is able to correctly associate each loop closure to one of the first 100 images in the dictionary (initial 512 entries correspond to noise bases). At each revisit, we can see diagonal lines associating the current image to one of the corresponding first 100 images. Fig. 11(b) shows a zoomed-in version, in which the initial noisy reconstruction during the first 100 images can also be seen, since at that time there are no valid loop closures present in the dictionary. It can be clearly seen from Fig. 11 that even in the case of 60 revisit, the proposed method is able to associate the current image to the first occurrence of the bases in the dictionary. This can be attributed to the greedy nature of the ℓ_1 -optimizer incorporated in the framework. It chooses the first basis that it can find which has the least reconstruction error according to (7), which in this case corresponds to the first occurrence of the basis in the dictionary. The existence of exact basis leads to minimization of the reconstruction error at the first step, hence returning the first occurrence of the corresponding basis.



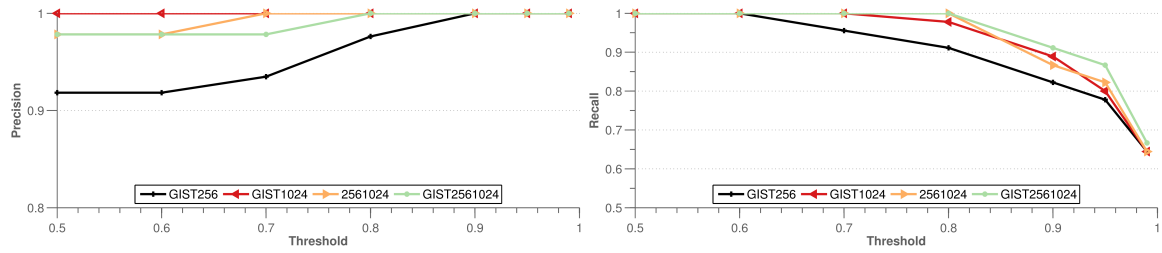
(a) Sequence 00



(b) Sequence 02



(c) Sequence 05



(d) Sequence 06

Figure 10: Precision and recall statistics of the proposed loop closing approach with multi-modal features on the KITTI visual odometry benchmark. Please note that the Y-axis for the Precision starts at 0.8 to make the details visible.

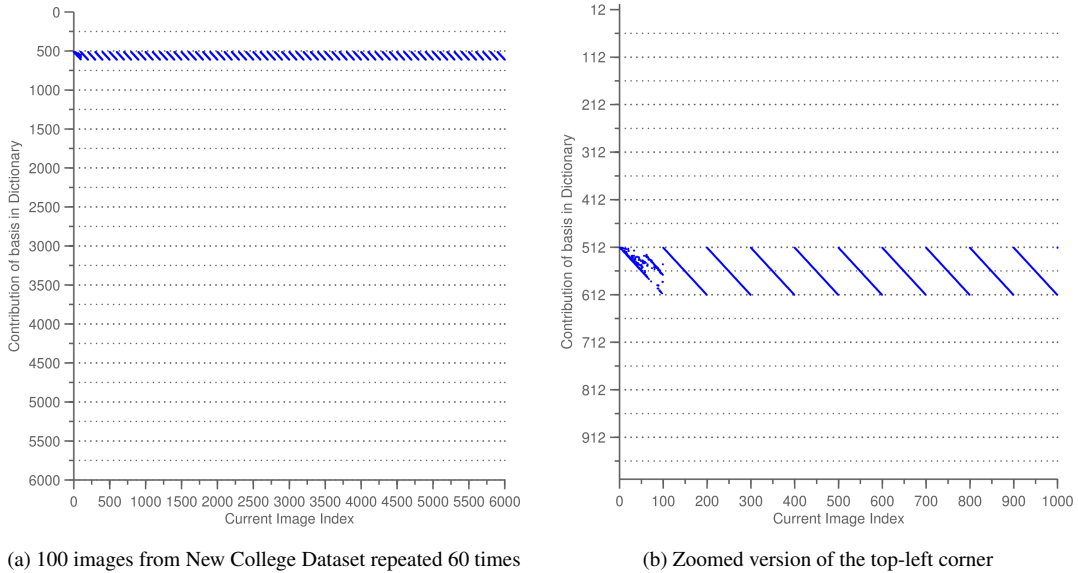


Figure 11: Revisit scenario using images from the New College Dataset: GIST descriptor is used as the feature of each image. All the images are presented 60 times to the proposed method for loop closure detection. Plots show the location of non-zero elements returned by the sparse optimization. Diagonal line segments correspond to loop closures.

5.7. Severe Illumination Changes

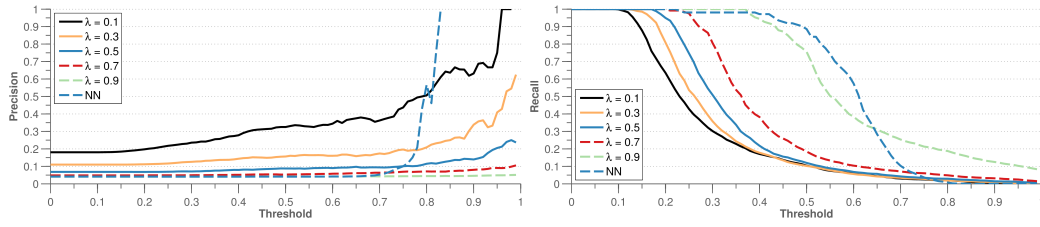
One of the challenges that makes place recognition difficult is illumination variation arising during long-term operation such as transitions from day to night or between different seasons. In order to test the performance of the proposed method under such severe illumination changes, we use the data from the Visual Place Recognition in Challenging Environments (VPRiCE) challenge [43]. The dataset consists of 7778 images from a variety of outdoor environments and under various viewing conditions. The dataset provides both *memory* and *live* images, and the objective is to find a match for each live image in the memory images. The first part of the dataset contains images acquired from a camera on-board a train, recorded in spring and winter for the same trajectory of the train, an example of which is shown in Fig. 12. In this test, we use only the images from the train sequences (2289 in memory and 2485 in live). The following experiments aim to investigate two aspects of the loop-closure problem: (i) the performance of the proposed method in challenging condition against a baseline of nearest-neighbor (NN) with exhaustive search, and (ii) the effect of the λ parameter on the sparsity of the solution.



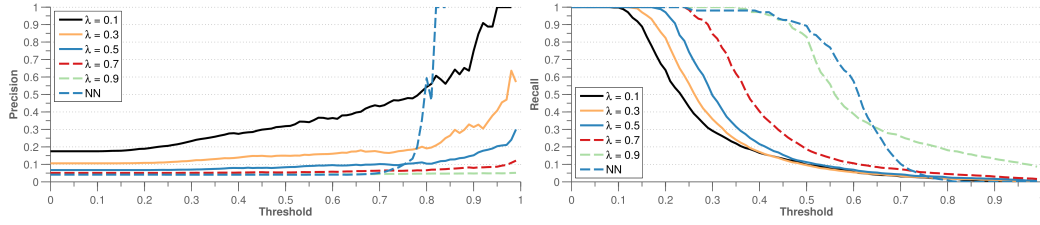
Figure 12: Example images from the VPRiCE challenge dataset where images have been acquired over different seasons.

To that end, we use two representations as mentioned earlier: the down-sampling raw images and the GIST descriptors. Each frame in *memory* is used to populate the dictionary and then a match is search for each *live* image. Note that no temporal or geometric consistency is applied and all decisions are taken just on the current image. Similarly, for each live image, we find the nearest neighbour match using an *exhaustive* search over *all* the memory images given the representation. The results are shown in Fig. 13. It can be seen that the proposed method provides better precision and recall in almost all the cases, and especially, the recall degrades more gracefully compared to the NN method. As opposed to the previous results, the threshold in Fig. 13 varies from 0 to 1 so that the results from the NN can be shown as well. Fig. 13 also shows that a smaller λ (a less sparse solution) leads to a higher precision but lower recall and vice versa, which agrees with the results in Fig. 5.

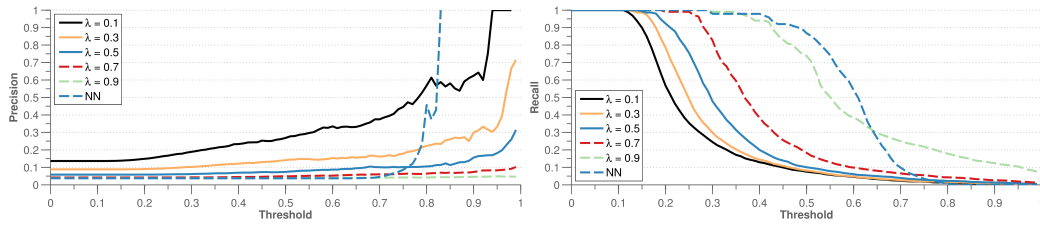
Another interesting aspect of the problem is the change in sparsity by varying λ . We report percentage of the number of nonzeros (NNZ) for different values of λ in Fig. 14 for the experiments presented in Fig. 13. As the value of λ increases, the solution become more sparse but even for smaller values the sparsity is a very small percentage of the number of vectors in the dictionary. The NN-based method, on the other hands, has all non-zeros entries corresponding to the number of vectors in the dictionary. These results imply that a sparse solution can be constructed even for small values of λ and the solutions is still much sparser as compared to the NN solution.



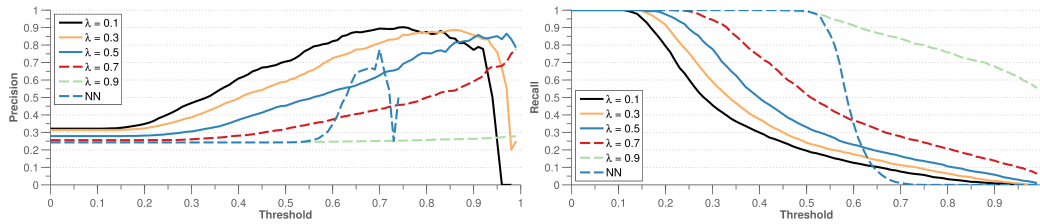
(a) Representation : Scaled by 1/8



(b) Representation : Scaled by 1/16



(c) Representation : Scaled by 1/32



(d) Representation : GIST

Figure 13: Performance Comparison on Norland Dataset: For NN, the x-axis corresponds to $1 - \text{distance}$. Varying the explanation penalty (λ) leads to better loop closure detection, but at the same time, the trade-off between precision and recall can be seen from the two plots. Better precision occurs are lower values of λ which has the effect of lower recall and vice versa.

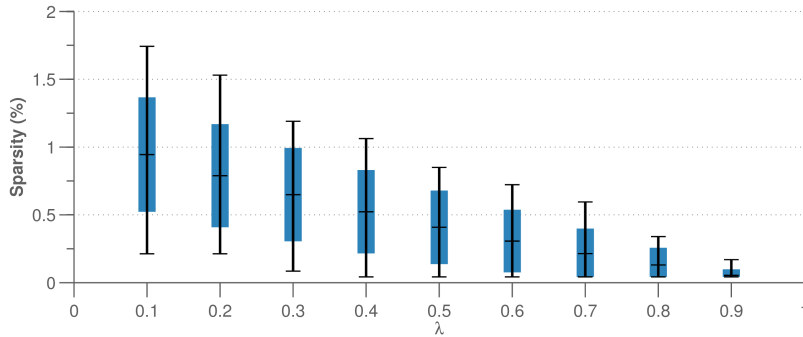


Figure 14: Analysis of the sparsity relationship with varying λ . Black vertical bars represent max, mean and min for each value of λ , while the blue bar spans mean with two standard deviations. The dictionary contains over 2000 vectors for this dataset.

6. Conclusions and Future Work

While the problem of loop closure has been well studied in visual navigation, motivated by the sparse nature of the problem (i.e., only a small subset of past images actually close the loop with the current image), in this work, we have for the first time ever posed it as a sparse convex ℓ_1 -minimization problem. The *globally optimal* solution to the formulated convex problem, by construction, is *sparse*, thus allowing efficient generation of loop-closing hypotheses. Furthermore, the proposed formulation enjoys a *flexible* representation of the basis used in the dictionary, with *no* restriction on how the images should be represented (e.g., what descriptors to use). Provided any type of image vectors that can be quantified with some metric to measure the similarity, the proposed formulation can be used for loop closing. Extensive experimental results have validated the effectiveness and efficiency of the proposed algorithm, using either the whole raw images as the simplest possible representation or the high-dimensional descriptors extracted from the entire images including feature from deep neural networks. We have also shown empirically how the design parameters effect the performance of our method, and in general, the proposed approach is able to efficiently detect loop closing for real-time applications. The quality of loop closure depends on the type of descriptor employed for the task. Raw images do not provide view-point or illumination invariance. For detecting loop closures in drastically different illumination conditions such as day and night, the problem is reduced to finding a suitable descriptor and then the proposed framework can be employed.

We currently use a single threshold τ to control the loop-closure hypotheses, which guarantees a globally unique hypothesis. However, in the case of multiple revisits to the same location, this hard thresholding

would prevent detecting any loop closures and the revisits would be simply considered as perceptual aliasing, which is conservative but loses information. In the future, we will investigate different ways to address this issue. For example, as mentioned earlier, we can sum up the contributions of basis vectors if a loop has already been detected between them and thus ensure that multiple visits lead to more robust detection of loop closures. Nevertheless, this has not been a major issue in our tests; as shown in Fig. 2 and Fig. 11, the proposed algorithm is capable of detecting loops at different revisits, even in the worst case scenario. As briefly mentioned before, the number of basis vectors in the dictionary grows continuously and can prohibit the real-time performance for large-scale problems. To mitigate this issue, one possible way would be to update the dictionary dynamically by checking a novelty factor in terms of how well the current image can be explained by the existing dictionary, which is akin to adding “key frames” in visual SLAM.

Acknowledgments

This work was partially supported by the MINECO-FEDER project DPI2015-68905-P, by the research grant BES-2010-033116, by the travel grant EEBB-I-13-07010, by the ONR grants N00014-10-1-0936, N00014-11-1-0688 and N00014-13-1-0588, by the NSF awards IIS-1318392 and IIS-15661293, and by the DTRA award HDTRA 1-16-1-0039.

References

- [1] E. Amaldi and V. Kann. On the approximability of minimizing nonzero variables or unsatisfied relations in linear systems. *Theoretical Computer Science*, 209(12):237–260, 1998.
- [2] M. Asif. Primal dual pursuit: A homotopy based algorithm for the Dantzig selector. Master’s thesis, Dept. of Electrical and Computer Engineering, Georgia Institute of Technology, 2008.
- [3] F. Bach, R. Jenatton, J. Mairal, and G. Obozinski. Convex optimization with sparsity-inducing norms. *Optimization for Machine Learning*, pages 19–53, 2011.
- [4] Y. Bengio. Deep learning of representations for unsupervised and transfer learning. *Unsupervised and Transfer Learning Challenges in Machine Learning*, 7:19, 2012.
- [5] S. Boyd and L. Vandenberghe. *Convex Optimization*. Cambridge University Press, 2004.

- [6] M. Calonder, V. Lepetit, C. Strecha, and P. Fua. BRIEF: Binary Robust Independent Elementary Features. In *European Conference on Computer Vision (ECCV)*, pages 778–792. Springer, Crete, Greece, 2010.
- [7] C. J. Cannell and D. J. Stilwell. A comparison of two approaches for adaptive sampling of environmental processes using autonomous underwater vehicles. In *MTS/IEEE OCEANS*, pages 1514–1521, Washington, DC, Dec. 19–23, 2005.
- [8] F. Capezio, F. Mastrogiovanni, A. Sgorbissa, and R. Zaccaria. Robot-assisted surveillance in large environments. *Journal of Computing and Information Technology*, 17(1):95–108, 2009.
- [9] J. J. Casafranca, L. M. Paz, and P. Pinies. ℓ_1 Factor Graph SLAM: going beyond the ℓ_2 norm. In *Robust and Multimodal Inference in Factor Graphs Workshop, IEEE International Conference on Robots and Automation, (ICRA)*, Karlsruhe, Germany, 2013.
- [10] J. J. Casafranca, L. M. Paz, and P. Pinies. A back-end ℓ_1 norm based solution for factor graph SLAM. In *IEEE/RSJ International Conference on Intelligent Robots and Systems (IROS)*, pages 17–23, Tokyo, Japan, Nov. 3–8, 2013.
- [11] B. Cheng, J. Yang, S. Yan, Y. Fu, and T. Huang. Learning with ℓ_1 -graph for image analysis. *IEEE Transactions on Image Processing*, 19(4):858–866, 2010.
- [12] W. Churchill and P. Newman. Experience-based navigation for long-term localisation. *The International Journal of Robotics Research*, 32(14):1645–1661, 2013.
- [13] M. Cummins and P. Newman. FAB-MAP: Probabilistic Localization and Mapping in the Space of Appearance. *The International Journal of Robotics Research*, 27(6):647–665, 2008.
- [14] N. Dalal and B. Triggs. Histograms of oriented gradients for human detection. In *IEEE Computer Society Conference on Computer Vision and Pattern Recognition (CVPR)*, volume 1, pages 886–893, San Diego, CA, June 20–26, 2005.
- [15] D. L. Donoho. Compressed sensing. *IEEE Transactions on Signal Processing*, 52(4):1289–1306, 2006.
- [16] D. L. Donoho. For most large underdetermined systems of linear equations the minimal 1-norm solution is also the sparsest solution. *Communications on pure and applied mathematics*, 59(6):797–829, 2006.

- [17] D. L. Donoho and Y. Tsaig. Fast solution of ℓ_1 -minimization problems when the solution may be sparse. Technical report, Dept. of Statistics, Stanford University, 2006.
- [18] M. Elad and M. Aharon. Image denoising via sparse and redundant representations over learned dictionaries. *IEEE Transactions on Image Processing*, 15(12):3736–3745, 2006.
- [19] M. Elad, M. Figueiredo, and Y. Ma. On the role of sparse and redundant representations in image processing. *Proceedings of the IEEE*, 98(6):972–982, 2010.
- [20] M. Everingham, L. Van Gool, C. K. I. Williams, J. Winn, and A. Zisserman. The PASCAL Visual Object Classes Challenge 2012 (VOC2012) Results. <http://www.pascal-network.org/challenges/VOC/voc2012/workshop/index.html>, 2012.
- [21] D. Galvez-Lopez and J. D. Tardos. Bags of binary words for fast place recognition in image sequences. *IEEE Transactions on Robotics*, 28(5):1188–1197, 2012.
- [22] A. Geiger, P. Lenz, and R. Urtasun. Are we ready for autonomous driving? the KITTI vision benchmark suite. In *Computer Vision and Pattern Recognition (CVPR), 2012 IEEE Conference on*, pages 3354–3361. IEEE, 2012.
- [23] V. Kumar B G, G. Carneiro, and I. Reid. Learning local image descriptors with deep siamese and triplet convolutional networks by minimising global loss functions. In *The IEEE Conference on Computer Vision and Pattern Recognition (CVPR)*, June 2016.
- [24] Y. Latif, C. Cadena, and J. Neira. Robust loop closing over time for pose graph SLAM. *The International Journal of Robotics Research*, 32(14):1611–1626, 2013.
- [25] Y. Latif, C. Cadena, and J. Neira. Robust graph slam back-ends: A comparative analysis. In *Intelligent Robots and Systems (IROS 2014), 2014 IEEE/RSJ International Conference on*, pages 2683–2690. IEEE, 2014.
- [26] Y. Latif, G. Huang, J. Leonard, and J. Neira. An online sparsity-cognizant loop-closure algorithm for visual navigation. In *Proceedings of Robotics: Science and Systems*, Berkeley, USA, July 2014.
- [27] Y. LeCun and Y. Bengio. Convolutional networks for images, speech, and time series. *The handbook of brain theory and neural networks*, 3361(10), 1995.

- [28] J. H. Lee, G. Zhang, J. Lim, and I. H. Suh. Place recognition using straight lines for vision-based SLAM. In *Robotics and Automation (ICRA), 2013 IEEE International Conference on*, pages 3799–3806. IEEE, 2013.
- [29] J. H. Lee, S. Lee, G. Zhang, J. Lim, W. K. Chung, and I. H. Suh. Outdoor place recognition in urban environments using straight lines. In *2014 IEEE International Conference on Robotics and Automation (ICRA)*, pages 5550–5557, May 2014.
- [30] S. Lowry, N. Sünderhauf, P. Newman, J. J. Leonard, D. Cox, P. Corke, and M. J. Milford. Visual place recognition: A survey. *IEEE Transactions on Robotics*, 32(1):1–19, 2016.
- [31] D. M. Malioutov, M. Cetin, and A. S. Willsky. Homotopy continuation for sparse signal representation. In *IEEE International Conference on Acoustics, Speech, and Signal Processing*, 2005.
- [32] M. Milford. Vision-based place recognition: how low can you go? *The International Journal of Robotics Research*, 32(7):766–789, 2013.
- [33] M. Milford and G. Wyeth. SeqSLAM: Visual route-based navigation for sunny summer days and stormy winter nights. In *IEEE International Conference on Robotics and Automation (ICRA)*, pages 1643–1649, St. Paul, MN, May 14–18, 2012.
- [34] D. Nister and H. Stewenius. Scalable recognition with a vocabulary tree. In *Computer Vision and Pattern Recognition, 2006 IEEE Computer Society Conference on*, volume 2, pages 2161–2168, 2006. doi: 10.1109/CVPR.2006.264.
- [35] A. Oliva and A. Torralba. Modeling the shape of the scene: A holistic representation of the spatial envelope. *International Journal of Computer Vision*, 42(3):145–175, 2001.
- [36] R. Paul and P. Newman. Self-help: Seeking out perplexing images for ever improving topological mapping. *The International Journal of Robotics Research*, 32(14):1742–1766, 2013.
- [37] RAWSEEDS. Robotics advancement through Webpublishing of sensorial and elaborated extensive data sets (project FP6-IST-045144), 2009.
- [38] E. Rosten and T. Drummond. Fusing points and lines for high performance tracking. In *IEEE International Conference on Computer Vision (ICCV)*, volume 2, pages 1508–1515, Beijing, China, Oct. 17–20, 2005.

- [39] M. Shakeri and H. Zhang. Online loop-closure detection via dynamic sparse representation. *Field and Service Robotics (FSR)*, 2015.
- [40] J. Sivic and A. Zisserman. Video Google: A text retrieval approach to object matching in videos. In *Proceedings of the International Conference on Computer Vision*, volume 2, pages 1470–1477, Oct. 2003.
- [41] M. Smith, I. Baldwin, W. Churchill, R. Paul, and P. Newman. The new college vision and laser data set. *The International Journal of Robotics Research*, 28(5):595–599, 2009.
- [42] H. Sugiyama, T. Tsujioka, and M. Murata. Collaborative movement of rescue robots for reliable and effective networking in disaster area. In *International Conference on Collaborative Computing: Networking, Applications and Worksharing*, San Jose, CA, Dec. 19–21, 2005.
- [43] N. Sünderhauf. Visual Place Recognition in Challenge Environments (VPRiCE) Challenge. <https://roboticvision.atlassian.net/wiki/pages/viewpage.action?pageId=14188617>, 2015.
- [44] N. Sünderhauf, F. Dayoub, S. Shirazi, B. Upcroft, and M. Milford. On the performance of convnet features for place recognition. In *Proc. IEEE/RJS Int. Conference on Intelligent Robots and Systems*, 2015.
- [45] N. Sunderhauf, S. Shirazi, A. Jacobson, F. Dayoub, E. Pepperell, B. Upcroft, and M. Milford. Place recognition with convnet landmarks: Viewpoint-robust, condition-robust, training-free. *Proceedings of Robotics: Science and Systems XII*, 2015.
- [46] H. Zhang, F. Han, and H. Wang. Robust multimodal sequence-based loop closure detection via structured sparsity. In *Proceedings of Robotics: Science and Systems*, AnnArbor, Michigan, June 2016. doi: 10.15607/RSS.2016.XII.043.